Surface salinity variability in the North Atlantic during recent decades

Sirpa Häkkinen,

NASA Goddard Space Flight Center,

Code 971, Greenbelt, MD 20771

January 2001

Abstract

The sea surface salinity (SSS) variability in the North Atlantic is investigated using numerical model simulations for the last 50 years based on atmospheric forcing variability from Comprehensive Atmosphere Ocean Data Set (COADS) and National Center for Environmental Prediction / National Center for Atmospheric Research (NCEP/NCAR) Reanalysis. The largest interannual and longer term variability occurs in two regions: the Labrador Sea and the North Equatorial Countercurrent (NECC) region. In both regions the seasonality of the surface salinity variability is prominent with the maximum standard deviation occurring in the summer/fall period. In the Labrador Sea the summer SSS anomalies far exceed those of wintertime in amplitude. The interannual SSS variability in the subpolar gyre can be attributed to two factors: excess ice melt and heat flux (i.e. deep mixing) variations. On the other hand, heat flux variability can also lead to meridional overturning changes on decadal time scales such that weak overturning is manifested in fresh surface conditions in the subpolar gyre. The overturning changes also influence the NECC region SSS variability. Moreover, the subpolar freshening events are expected to occur during the negative phase of North Atlantic Oscillation which is associated with a weak wintertime surface heat loss in the subpolar gyre. No excess sea ice melt or precipitation is necessary for the formation of the fresh anomalies, because with the lack of wide-spread deep mixing, the fresh water that would be expected based on climatology, would accumulate at the surface. Thus, the fresh water 'conveyor' in the Atlantic operates via the overturning circulation such that deep mixing inserts fresh water while removing heat from the water column.

1. Introduction

North of 40°N and south of 40°S, there is net precipitation over evaporation. This fact must be reconciled in the closure of the global salinity budget to understand the surface salinity distribution and its variability. Assuming that the total fresh water resources are nearly in equilibrium, i.e. no major accumulation or depletion over the ice sheets occurs, the question arises how does this 'excess' fresh water return to the lower latitudes where it can again evaporate and be transported by the atmosphere to the higher latitudes ? In the North Atlantic there are no major surface ocean currents that transport the cold and fresh waters from the polar/subpolar oceans to the latitudes around 20N where most of the evaporation takes place. Certainly, the 'fresh' coastal current along the eastern seaboard in the North Atlantic cannot penetrate southward due to the blockage by the Gulf Stream. During summertime subpolar waters are known to spread southward in the north-eastern side of the basin and to be eventually mixed down and subducted in the following winter (Bauer et al. 1991). Thus, no effective surface route exists for southward fresh water transport, so the only route back to the lower latitudes has to take place through the meridional circulation. The subpolar/polar regions are source regions for the intermediate and deep/bottom waters, thus a part of the fresh water route back to global system coincides with the thermohaline circulation. In the present climate the conversion of light water to bottom water in the North Atlantic occurs mainly through heat loss rendering the opposing fresh water (haline) flux less important.

Wide spread fresh anomalies in the surface salinity in the northern North Atlantic have been occurring nearly once a decade (Reverdin et. al. 1997, Belkin et al. 1998). Individual 'fresh' events vary considerably from location to another, but by far the largest and most wide spread occurrence was the Great Salinity Anomaly (GSA) at the end of 1960's and early 1970's (Dickson et al 1988). Another large event took place in the early 1980' (Belkin et al. 1998). These events serve as a reminder about the delicate balance between the thermal and haline component of the surface buoyancy flux. Dickson et al 1988

estimated the excess fresh water associated with this event to be about 2300 km^3 (equals to about 4 times the transport of the Mississippi River). Observational studies by Levitus (1989a,b) have documented the widespread influence of the GSA in the hydrography of the N. Atlantic by comparing pentads of 1955-1959 and 1970-1974. Also the event led to a cessation of convection in the Labrador Sea as recorded at weather station Bravo (Lazier, 1980). Diagnostic studies by Greatbatch et al (1991) and Ezer et al (1995) have investigated the dynamic influence of the changes in hydrography between the above mentioned pentads before and after the GSA. They have shown that there was a considerable decrease in the strength of the subtropical gyre (a decrease of 30Sv). This change is associated with a decrease in the north-south sea level tilt (Ezer et al 1995) as observed at coastal tide gauges. Diagnostic studies are not capable of estimating changes in the meridional heat transport and are thus inconclusive. However, a prognostic ocean simulation (Häkkinen, 1999a) shows that the late 1960's and early 1980's were also time periods of weakened overturning and meridional heat transport.

When searching for causes of the salinity anomalies in the subpolar gyre, it is necessary to consider both the haline and thermal component of the surface buoyancy flux. The haline component has received more attention for the apparent reason that the melt water from ice sheets is a potentially overwhelming source of fresh water at high latitudes; presently the Greenland ice sheet ablation (=snow accumulation) is about 500km^3 per year. However, this is a small amount compared to the annual sea ice export from the Arctic, 2000-2800km^3 on average which is about the same volume as the river runoff to the Arctic Basin. On the seasonal and interannual scales the variability of the sea ice export from the Arctic can be effective in redistributing fresh water: modifying the surface water masses and mixing processes and consequently the thermohaline forcing at high latitudes. This variability affects deep waters as well as mode waters (intermediate water masses) which can have a climatic impact on decadal time scale because they will come into contact with the atmosphere much faster than the deep waters. Furthermore, numerical modeling of the Arctic/GIN Seas system

has shown that the variability in the sea ice transport from the Arctic can be nearly as large as the mean (Häkkinen, 1993; 1995). Although, high latitudes are characterized by net precipitation, the sea ice melt adds an important contribution to the surface fresh water flux, and, depending on location, it can even be the main contributor to the total surface buoyancy flux. Thus, if the ice/fresh water is injected into the system in areas of deep mixing, the water mass densification can be disturbed. The modeling results (Häkkinen, 1993; 1999b) suggest that the GSA may have had a considerable contribution from excess sea ice transported from the Arctic.

The fresh surface conditions in the subpolar gyre tend to occur in conjunction with weak loss (Dickson et al. 1996). The weak heat loss is typical of years with the negative phase of the North Atlantic Oscillation (NAO) which describes a weak Icelandic Low and a weak Azores High. NAO effectively modulates deep convection in the Labrador Sea with the Labrador Sea Water as the end product (Marshall and Schott, 1999). Lack of thermally driven convection leaves the local precipitation (and sea ice melt water etc.) at the surface which would be normally mixed down during the formation of deep winter mixed layer. Thus, the thermal component of the buoyancy flux can be equally important in creating fresh surface conditions in the northern North Atlantic. This process is considered here as the main cause of the decadally occurring fresh surface salinity anomalies. This study will examine how we can link the observed fresh salinity anomalies in the subpolar gyre to a weakened heat loss which also means weakened overturning at the same time. However, it is expected that at shorter interannual time scales the influence from the ice export should be also evident. This paper is divided as follows: Section 2 describes the model and its forcing. To establish the model performance in reference to observations Section 3 first discusses how the sea surface salinity (SSS) varies seasonally and then its longer variability. Sections 4 and 5 discusss SSS variability in association with meridional overturning and ice export variability.

2. Ocean model description and its forcing

The ocean model is hydrostatic and Boussinesq and uses the sigma-coordinate system as described in Blumberg and Mellor (1987) with a modified scalar advection scheme to avoid overshooting at sharp fronts (Mauritzen and Häkkinen, 1997). The 2.5 level turbulence closure scheme of Mellor and Yamada (1982) is used to determine the vertical mixing coefficients for momentum and scalar variables. The dynamic-thermodynamic ice model is coupled to the ocean model via interfacial stresses and via salinity and heat fluxes through the ice-water interface. The ice model uses a generalized viscous rheology as discussed in Häkkinen and Mellor (1992).

The coupled ice-ocean model extends from the Bering Strait to 15°S with resolution of 7/10° in 'longitude', 9/10° in 'latitude' (in a rotated coordinate system with equator at 30°W and the pole at (120°W, 0°N). There are a total of 20 sigma-levels in the vertical with higher resolution near the surface. To minimize the inaccuracies in the computation of the pressure gradient, the topography (derived from the TerrainBase Global DTM data base with 5'x5' resolution) is smoothed heavily. However, the Nordic sills were kept with depth of 650 m at Denmark Strait and of 1100 m at the Faeroe-Shetland Channel.

The initialization of the hindcast simulation is taken from the end of the 10th simulation year of a quasi-equilibrium runs presented in Mauritzen and Häkkinen (1997). The quasi-equilibrium run was initialized with the annual average hydrographic climatology of Levitus et al. (1994). The transports at oceanic lateral boundaries were specified to be 0.8Sv through the Bering Strait, and 0.8Sv out at 15°S. At the southern boundary the salinities and temperatures are relaxed to Levitus values in 5 grid rows from the boundary. Restoring of T and S is also used at the Mediterranean outflow point. The water masses in the upper ocean and just below the permanent thermocline (e.g. Labrador Sea Water) have time scales of a decade (Rossby wave transmission in the model mid-latitudes is 6 years across the basin). Thus, the decadal variability and deep ocean time scales are rather well separated and one can consider the decadal variability superimposed on the slower deep

ocean variability. The same model results concerning the meridional heat transport, overturning and their atmospheric forcing are discussed in Häkkinen (1999a).

The model is forced with atmospheric climatological data for the first 10 years, after which COADS anomalies (1946-1993) (daSilva et al. 1994) are added to the atmospheric forcing. The simulation using anomalies from NCEP/NCAR Reanalysis (1958-1999) is initiated from December of 1957 of the COADS simulation. The cloudiness and the precipitation minus evaporation (P-E) field and river runoff are climatological throughout both simulations. For the heat exchange the bulk formulation is adopted where the heat fluxes are a function of the oceanic surface quantities. The heat exchange with coefficient of 1.3×10^{-3} is used regardless of air-ocean stability conditions. The surface mixing ratio is computed from model generated surface temperature with 98% saturation. The model SST is also used in the upward longwave radiation.

The model simulated data are monthly averaged, and only the years 1951 through 1993 are used as in Häkkinen (1999a). All years (1958-1999) from the NCEP/NCAR simulation are used although the transition from COADS to NCEP/NCAR is not smooth. The model simulation displays a quadratic trend on which the decadal variability superimposed. Since we are not interested in the trend, we simply remove a quadratic trend in every grid point, unless otherwise specified.

3. Sea Surface Salinity variations

3.1 Overview of Seasonal variability

To understand long term SSS variations, the seasonal cycle of the simulated SSS is first established in comparison to the climatological data (Levitus et al.1994, Levitus 1989b). The annual average SSS from the observations and model are shown in Figs. 1a-b. The model produces a reasonably realistic SSS field in comparison with observations. Particularly the subtropical maximum is well reproduced. The spatial distribution of seasonal variance from the climatology and from the model are shown in Figs. 2a-b. The largest

seasonal variability is concentrated in the subpolar gyre and in the Northern Equatorial Countercurrent (NECC). In the subpolar gyre the seasonal SSS depends on the temporal variability of the local fresh water input, the precipitation minus evaporation balance (P-E) and ice melt (and advection of fresh waters away from the coastal areas). In the area NE off Brazil, the spreading of the Amazon plume is controlled by the seasonal variations of NECC.

To understand possible sensitivities of the SSS behavior on longer times scales in the subpolar gyre, an areal average (40N-60N, 60W-40W; ice-covered areas excluded; this definition will be used throughout the paper when referring to the subpolar gyre), seasonal SSS from the model and from the Levitus climatology are shown in Fig. 3. The model SSS is somewhat more saline than the observed climatology. Considering the sharp gradient of SSS towards the coasts (Figs. 1), the spreading of the coastal fresh waters is not as effective in the model as in the nature which may be the main reason that the model exhibits somewhat more saline values. However, the shift in the absolute value should not influence significantly the variability itself as can be seen from the very reasonable seasonal standard deviation of the SSS when compared to observations (Figs. 2). To explain, at least partly, the timing of the SSS minimum, the comparison with the seasonal P-E is displayed together with the simulated SSS (Fig. 3). Two local minima of P-E occur at late winter and at fall. The winter minimum lasts from February until June-July when P-E abruptly doubles. The annual P-E (about 1300km3) over the area competes with the net ice export through the Denmark Strait of about 1000 km3 (Hakkinen and Geiger, 2000). The significant aspect of the seasonal cycle is the fact that there is always a strong freshening in the late summer due to the climatological fresh water input whether it be P-E, sea ice melt water, or fresh water advection from the subpolar coastal region in general.

3.2 Non-seasonal SSS variability in the subpolar gyre

The spatial distribution of the non-seasonal SSS standard deviation (SD) is depicted in Figs. 4. Again the subpolar gyre and the Amazon plume area appear with the largest

variability. By using high and low pass Hanning filtering these values are divided into the variability shorter than 4 years (interannual; IA) and longer than 4 years (low-frequency; LF) (Fig. 4b-c). The values shown in Fig. 4c for the LF component represent typically 30-50% of the total non-seasonal monthly SD. The simulated values compare well with SD computed for the station data of Reverdin et al. (1997) which span the subpolar gyre.

The simulated monthly distribution of the SSS standard deviation in the subpolar gyre displays a strong seasonal dependence (Fig. 5). In winter, the subpolar SSS has the least variability, while the high variability is concentrated in summer and fall. August and September constitute the center of a broad maximum. The limited surface observations suggest also that the observed SD reaches maximum in early fall of which the salinity variability at Ocean Weather Station Bravo (Lazier, 1980) gives a good example. To emphasize the disparity of the winter and summer SSS anomalies in the subpolar gyre, the simulated anomalies for March and August are shown in Fig.6a and 6b for the model runs forced by COADS and NCEP/NCAR Reanalysis anomalies respectively. Overall the simulated variability compares quite well with the observations recording the fresh events of early 1970's (GSA) and 1980's (Belkin et al. 1998). The Reanalysis simulation captures better a strong and long lasting SSS minimum during the GSA period when compared to the COADS simulation, but the latter appear to reproduce a well-defined minimum in the early 1980's with the Reanalysis simulation somewhat lacking in strength. The strong freshening in the beginning of 1950's maybe also a realistic feature because observations show that the Labrador Current was very fresh at that time (Petrie and Drinkwater, 1993). The NCEP/NCAR simulation suggests a considerable freshening in the latter part of 1990's. The freshening of the upper layers since 1996 has been observed during the German field program on "Convection and Deep Water Formation in the Labrador Sea" (F. Schott, Private communication, 2001). During the same time period the investigation of the hydrographic observations between Newfoundland and Iceland (Reverdin et al. 1999) reports salinization in the northern part of the section which falls mostly outside of the subpolar region

investigated in this study. As apparent from Reverdin et al. (1997) the observed freshening events are very sensitive to the location. This is true also for the simulated events, however, the timing of the fresh events themselves is reproduced in the simulations.

3.3 Mixed layer depth variability in the subpolar gyre

In the following the modulation of deep mixing in the subpolar gyre is considered as the primary reason for the appearance of the decadal fresh events which are rather well reproduced in the model even though P-E is set to the seasonal climatology throughout the simulation. The hypothesis is that with a weakening of the wintertime surface heat loss, mixing diminishes and will result in a shallow and fresh mixed layer by the end of the winter season. Since the ice melt and the largest P-E occur in the summer, the local fresh water sources will further amplify the fresh surface salinity signal towards the end of summer. Hence, no outside excess fresh water source is necessary to produce the freshening events. This does not mean that the outside sources could not participate , to amplify or to diminish, at least some of the fresh events, e.g. to GSA, but the coincidence of the winter heat flux anomaly and (subsequent) summer fresh anomaly suggests that winter processes bear the main role. Here the heat flux variability is not dealt explicitly, as the subpolar mixed layer depth at the extremes of the heat flux variability is shown Häkkinen (2000). The more general relationship between heat flux and overturning is discussed in Häkkinen (1999a).

To explore the relationship between the winter mixing and summer SSS anomalies, the mixed layer depth is computed for the month of March which has normally the deepest mixed layer in the central subpolar gyre. A density difference of 0.05 sigma-t units at the bottom of the mixed layer is used as the criterion. The March mixed layer depth along with the August SSS anomaly (as an average 40N-60N, 60W-40W) from the same year are displayed in Fig. 7a (COADS simulation). In Figs. 7b and 7c the March mixed layer and August SSS anomalies are compared between the two simulations. The agreement between the two model runs is remarkable especially for the mixed layer depth. In 19 cases from 42

years, anomalies of the same sign in the mixed layer and SSS are present during the same year. If March mixed layer anomaly leads by one year, the occurrence of a SSS anomaly of the same sign increases to 26 cases from 41 years. With mixed layer depth anomaly leading by 2 years, the SSS anomaly of the same sign occurs in 20 cases from 40 possible years. On the other hand if the August SSS anomaly leads, the following March mixed layer depth is of the same sign in 21 cases from 41 years. The persistence of the SSS and mixed layer anomalies is intertwined, because once conditions where less deep mixing occurs, i.e. very fresh surface layers, there is a positive feedback to slow down further deep mixing in the following winter. As a result it will take several years to dissipate the SSS anomalies since there is no direct damping by the atmosphere. Clearly SSS-mixed layer depth variability is not a perfect match and the role of sea ice is discussed later on. Interestingly enough, the March SSS and mixed layer depth anomalies do not have a very strong relationship. Despite its weak amplitude, the winter (March) SSS has much stronger decadal variability than the summer SSS and autocorrelation stays high for lag= +/-1 year. The difference in behavior of winter and summer SSS in respect to winter mixed layer anomalies suggest other lower frequency processes, such as ocean circulation changes, determining mainly the winter SSS anomalies. The circulation changes provide the low frequency envelope to the summer anomalies also on which interannual variability arising from the sporadic ice export and deep convection events is superimposed.

As noted earlier the fresh anomalies may strongly depend on the location in the subpolar gyre, some events may not be distinguishable in all areas. To explore the SSS variability while at the same time suppressing the spatial dependence, the SSS anomalies (averaged for July-September) and winter mixed layer anomalies (averaged over January-March) exceeding one standard deviations are counted based on their population in the subpolar gyre. In this manner the large fresh and salty anomalies are accounted for as well as shallowing and deepening of the winter mixed layer even if they occupy different parts of the gyre at the same time. The distribution of grid points where the absolute value of the two

quantities at any given time exceed one SD is shown in Fig.8a and 8b for the COADS and Reanalysis forcing respectively. 100 gridpoints constitute an area of 630000km2 which corresponds to about 10 degrees of latitude times 10 degrees of longitude at 50N. As anticipated, the negative extrema population goes up, when the positive extrema population goes down. However, anomalies of both sign are present at times, especially in the early 1980's. The mixed layer depth and SSS anomaly population follow each other rather well, with a few occasions where salinity was significantly different like in the early 1970's and in 1979 when one can suspect contribution from the sea ice effects. Both simulations support the wide-spread cessation of mixing during 1970, with 1966 and 1999 (depending on the simulation) competing for the next largest occurrence.

3.4 Seasonal and non-seasonal variability in the NECC region

The other significant center of seasonal and non-seasonal SSS variability is in the northern tropics on the western side where the runoff from Amazon influences the surface conditions. The seasonal behavior of NECC in the western basin is such that it is the strongest in summer (July-September) and extends across the basin when the Intertropical Convergence Zone (ITCZ) is at its northernmost position (trades are weak with a southerly component) and disappears during winter/spring (January-May) when ITCZ is at its southernmost location (local trades are the strongest with a northerly component) (Richardson and Walsh, 1986). This seasonal variability of NECC determines that the Amazon waters would be advected eastward during summer, but would remain along the coast in the winter. The seasonal behavior of SSS in the region (65W-50W, 5N-15N; SSS(NECC)) follows closely this cycle (Fig. 9). Garzoli and Katz (1983) discuss the forced nature of the NECC seasonal variability by vorticity changes associated with the seasonal variability of the trades. A delay of 5-7 months between the thermocline changes in the east and west boundaries is found with an apparent propagation westward and enhancement by the local Ekman pumping in the western basin. The initiation of the thermocline anomalies in

the eastern boundary are tied to the wind stress vorticity changes. The baroclinic adjustment time scale to wind driven changes is several months at latitudes 4N-10N, hence the variability in the winter trades will influence the NECC and SSS in summer.

The non-seasonal standard deviation (also in Fig. 9) has a maximum in late summer and fall at the time when NECC is established in the western section of the northern tropics. This suggests that interannual and lower frequency variability in the NECC is responsible for the SSS variability. There is an anticipated linkage between the year-to-year changes in SSS(NECC) and in the northern trades: A cross-correlation between SSS(NECC) and the average zonal wind stress (5N-20N, 60W-20W) (-0.56; significant at 95% level) suggests that summer SSS (an average of July-September) and winter trades (an average of Jan-March) have an inverse dependence (positive SSS anomalies are related to negative stress anomalies , i.e. stronger trades). However, this is opposite to what one would expect based on the seasonal variability of the trades. Thus, low frequency changes in winter trades (directly or indirectly) have to be associated with large scale circulation changes leading to SSS variations in the NECC region. At the low frequencies the North Atlantic circulation variability involves the whole basin because of the large scale adjustment. Since the leading order circulation changes involve thermohaline processes (Häkkinen, 2000; Häkkinen and Mo, 2000), changes in NECC can be linked to the large scale variation of the thermohaline circulation and its impact on the horizontal gyre circulation. The composite surface salinity at the extrema of winter trades resembles Fig. 10b which is a composite SSS for meridional heat transport at 45N. This suggests that the non-seasonal SSS changes in the NECC region are not driven locally or by the tropical Atlantic atmospheric variability, but processes governing the whole North Atlantic Ocean.

4. Influence of the thermohaline circulation on SSS

Thermohaline processes can affect SSS in the northern North Atlantic in two ways, the first one related to lack of deep mixing has already been discussed, the other one relates to

the changes in the meridional transport of salt from the lower latitudes. Meridional heat transport is used here as a proxy for the meridional overturning strength. Since the largest SSS anomalies occur in the late summer (July-September), a composite SSS is formed based on the annual average anomaly of the meridional heat transport at 45N (MHT45) when the absolute value of MHT45 anomaly exceeds one standard deviation. At 0, a positive SSS anomaly begins to form in the subpolar gyre reaching maximum a year after the MHT45 maximum. At lags 0 and 1 the SSS anomaly covers a large portion of the subpolar gyre. The large positive anomalies are associated with warm SST anomalies extending southward along the Gulf Stream. Lacking any P-E anomalies in the simulation, the source of these anomalies is an increased advection from the south. As referred in the previous section, the thermohaline circulation has also a strong SSS signal in the tropical Atlantic in the NECC and North Equatorial Current areas.

Another way to explore the large scale circulation influence on SSS is to inspect the Empirical Orthogonal Function (EOF) decomposition of SSS which selects stationary patterns with the largest variances. Since SSS has very strong localized peaks, the SSS time series in each point were normalized by its SD. It turns out that only the first mode has a significant portion of variance associated with it (14%), remainder of the modes containing less than 5% of the variance. The spatial pattern of the first mode is shown in Fig 11a for the COADS simulation (Reanalysis results in a very similar EOF). The North Atlantic variability contains a tripole pattern with broad centers of alternating signs, a known pattern from SST variability (Deser and Blackmon, 1993). The smoothed annual average time series of this mode (PC1) and MHT45 show similar decadal variability (Fig. 11b) such that more saline conditions in the subpolar gyre are associated with strong overturning. Thus, decadal fresh and saline surface conditions in the subpolar gyre are associated with the variability of the meridional overturning where the heat flux forces the overturning (Häkkinen, 1999a).

SSS variations at decadal time scales are a consequence and not a cause of thermohaline variability despite the fact that SSS anomalies have a positive feedback with

overturning. The role of positive feedback is negated by the overwhelming contribution from thermal flux as the driver of overturning. In Fig. 11b the subpolar heat content (over the top 500 meters) anomalies are plotted along the SSS PC1 and MHT45 anomalies. The negative heat content anomalies precede the increased overturning and lead the SSS PC1 by 1-2 years. In fact there are no simultaneous correlation between the heat content and SSS PC1 (or with the subpolar SSS or upper ocean salinity content). If salinity would participate in the decadal overturning variability significantly, a correlation should exist between heat and salt content considering the potential of positive feedback between salinity and overturning.

5. Influence of the sea ice influx on the subpolar SSS

It was noted earlier that when the mixed layer depth variability and SSS do not always follow each other, excess sea ice in the subpolar gyre could be the culprit. The subpolar SSS anomaly (in an area always free of ice) averaged for August-October months and ice export anomaly through the Denmark Strait is depicted in Fig. 12 from the Reanalysis simulation. While there are broad tendencies that the positive ice export and negative SSS anomalies coincide, there is no clear relationship between the two on interannual or longer time scales. There are no significant correlations at any time scale between the two quantities. This is because the ice drift is wind driven which represents nearly white noise at the northern latitudes. Thus, sea ice can act as random modulator of the convection and surface conditions in the subpolar gyre. The influence of these random events is very short lived, less than a year, as can be gathered from a SSS composite based on Denmark Strait ice export (Fig. 13).

The role of ice export becomes significant if the excess events occur at the times of weak heat loss in the subpolar gyre as may have happened during the GSA. Fig. 12 indicates that in fact this was the only time period when the two were in-phase to support very fresh surface conditions. The excess fresh water was able to circulate around the subpolar gyre because the heat flux driven deep convection was minimal. The lack of deep

mixing was wide-spread because the spatial scale of the heat exchange spans the whole subpolar basin.

6. Conclusions

Based on model simulations the surface salinity variability in the North Atlantic has been explored. Two different forcings were used, one from COADS (daSilva et al. 1994) (1946-1993) and one from NCEP-NCAR Reanalysis (1958-1999). The model results were consistent with each other in the overlapping period. The Reanalysis was to used extend the model results up to the end of 1999, because apparently another very fresh surface anomaly has developed in the subpolar gyre since the mid-1990's. This anomaly is produced in the model results. The largest surface salinity variability is concentrated to two regions : the subpolar gyre (the Labrador Sea) and the NECC region such that the non-seasonal standard deviation of SSS reaches maximum in the late summer-early fall period.

In the Labrador Sea, the seasonality of the interannual and lower frequency variability is extreme with summer SSS anomalies far exceed those of wintertime in amplitude. However, the subpolar summer anomalies contain large interannual noise, some of which comes from variability in the local ice cover and ice export through the Denmark Strait. The interannual SSS variability can be attributed to two factors: excess ice melt and high frequency heat flux (deep mixing) variations (i.e. not all deep mixing events lead to meridional overturning changes which would require several years of diminished or increased local heat flux changes). The role of excess ice melt cannot be clearly separated because it can enhance or diminish the effects of the local heat flux. While the winter SSS anomalies are weaker, they have strong persistence suggesting large scale ocean circulation changes as the origin. The SSS anomalies also vary strongly with regions, not all fresh water events appear at all locations with similar magnitude. For instance, a composite of SSS at extremes of the meridional heat transport at 45N pinpoints an area limited to the southern half of the subpolar gyre. The maximum salinity differences reach 0.3psu when

July-Sept averages are used. The EOF analysis selects this area along with centers in the Amazon plume/NECC area and in the northern subtropics as the first mode. The time series associated with this spatial pattern explains only 14% of the total variance. The low frequency component of this time series correlates well with the overturning rate. Thus, by searching large scale SSS anomaly features one can extract information that can be related to overturning. However, on decadal time scales SSS is mainly a passive tracer of overturning changes, although at high latitudes it provides some positive feedback on shorter time scales by acting as preconditioning mechanism from the previous summer for the winter convection.

In summary, it is found that on decadal time scales SSS in the subpolar gyre and the tropical North Atlantic (NECC region) vary in unison. This covariability is associated with the changes in meridional overturning. Specifically, it is found that the low-frequency fresh surface conditions in the subpolar gyre are associated with changes in the local heat flux and meridional overturning as measured by the meridional heat transport at latitude 45N. This means that subpolar fresh surface conditions are expected to occur during the negative phase of NAO when the wintertime surface heat loss is weakened. No excess sea ice melt or precipitation is required for the formation of the fresh anomaly, because with the lack of deep mixing the fresh water that would be expected from climatology would accumulate at the surface. This implies that the fresh water conveyor in the Atlantic operates via the overturning circulation such that deep mixing inserts fresh water while removing heat from the water column.

Acknowledgments:

The support from NASA Headquarters for this work is gratefully acknowledged. I also thank Lena Marshak for the technical help with data and graphics.

References:

Bauer, J., H. Leach, and J.D. Woods: The seasonal variations of heat and fresh water contents between Azores and Greenland, *Q.J. R. Meteorol. Soc.*, 117, 1081-1104, 1991.

Belkin, I.M., S. Levitus, J. Antonov, S.-A. Malmberg: "Great Salinity Anomalies" in the North Atlantic, *Progress in Oceanography*, 41, 1-68, 1998.

Blumberg, A. F., and G. L. Mellor: A description of a three-dimensional coastal ocean circulation model. *'Three-Dimensional Coastal ocean Models'*, edited by N. Heaps. American Geophysical Union, 208 pp., 1987.

daSilva, A.M, C.C. Young, S. Levitus: Atlas of surface marine data 1994, Volume 1, Algorithms and procedures, NOAA Atlas Series. 1994.

Deser, C., and M.L. Blackmon: Surface climate variations over the North Atlantic Ocean during winter:1900-1989, *J. Climate*, 6, 1743-1753, 1993.

Dickson, R.R., J. Meincke, S.-A. Malmberg, A.J. Lee: The "Great Salinity Anomaly" in the northern North Atlantic, 1968-1982. *Progress in Oceanography*, 20, 103-151, 1998.

Dickson, R.R., J. Lazier, J. Meincke, P. Rhines, and J. Swift: Long-term coordinated changes in the convective activity of the North Atlantic, *Progress in Oceanography*, 38, 241-295, 1996.

Ezer, T., G.L. Mellor , and R.J. Greatbatch: On the interpendatal variability of the North Atlantic Ocean: Model simulated changes in transport, meridional heat flux and coastal sea level between 1955-1959 and 1970-1974, *J. Geophys. Res.*, 100, 10559-10566, 1995.

Greatbatch, R.J. , A.F. Fanning, A.D. Goulding, and S. Levitus: A diagnosis of interpendatal circulation changes in the North Atlantic, *J. Geophys. Res.*, 96, 22009-22023, 1991.

Garzoli S., and E.J. Katz: The forced annual reversal of the Atlantic North Equatorial Countercurrent, *J. Phys. Oceanogr.*, 13, 2082-2090, 1983.

Häkkinen, S. and G.L. Mellor: Modeling the seasonal variability of the coupled Arctic ice-ocean system, *J. Geophys. Res.*, 97, 20285-20304, 1992.

Häkkinen, S.: An Arctic source for the Great Salinity Anomaly: A simulation of the Arctic ice ocean system for 1955-1975, *J. Geophys. Res.*, 98, 16397-16410, 1993.

Häkkinen, S.: Simulated interannual variability of the Greenland Sea deep water mass formation and its connection to surface forcing, *J. Geophys. Res.*, 100, 4761-4770, 1995.

Häkkinen, S.: Variability of the simulated meridional heat transport in the North Atlantic for the period 1951-1993, *J. Geophys. Res.*, 104, 10991-11007, 1999a.

Häkkinen, S.: A simulation of thermohaline effects of a great salinity anomaly, *J. Climate*, 12, 1781-1795, 1999b.

Häkkinen, S. and C.A. Geiger: Simulated low-frequency modes of circulation in the Arctic Ocean, *J. Geophys. Res.*, 105, 6549-6564, 2000.

Häkkinen, S.: Decadal air-sea interaction in the North Atlantic based on observations and modeling results, *J. Climate*, 13, 1195-1219, 2000.

Häkkinen, S. and K.C. Mo: Low frequency variability of the tropical Atlantic Ocean, *J. Climate*, submitted, 2000.

Lazier, J.R.N.: Oceanographic conditions at Ocean Weather Ship BRAVO 1964-1974. *Atmosphere-Ocean*, 18, 227-238, 1980.

Levitus, S.: Interpendatal variability of temperature and salinity at intermediate depths of the North Atlantic Ocean, 1970-1974 versus 1955-1959, *J. Geophys. Res.*, 94, 6091-6131, 1989a.

Levitus, S.: Interpendatal variability of salinity in the upper 150 m of the North Atlantic Ocean, 1970-1974 versus 1955-1959, *J.Geophys. Res.*, 94, 9679-9685, 1989b.

Levitus, S., R. Burgett, and T.P. Boyer: World Ocean Atlas 1994, Vol.3: Salinity, NOAA Atlas NESDIS 3, U.S. Dept. of Commerce, Wash. D.C, pp 99. 1994.

Marshall, J. and F. Schott: Open-ocean convection: Observations, theory and models, *Rev. Geophys.*, 37, 1-64, 1999.

Mauritzen, C. and S. Häkkinen: Influence of sea ice on the thermohaline circulation in the Arctic-North Atlantic Ocean, *Geophys. Res. Lett.*, 24, 3257-3260, 1997.

Mellor, G.L. and T. Yamada: Development of a turbulence closure model for geophysical fluid problems, *Rev. Geophys.*, **20**, 851-875, 1982.

Petrie, B. and K. Drinkwater: Temperature and salinity variability on the Scotian Shelf and in the Gulf of Maine 1945-1990, *J. Geophys. Res.*, 98, 20079-20089, 1993.

Reverdin, G., D. Cayan, and Y. Kushnir: Decadal variability of hydrography in the upper northern Atlantic, 1948-1990, *J. Geophys. Res.*, 102, 8505-8532, 1997.

Reverdin, G., N. Verbrugge, and H. Valdimarsson: Upper ocean variability between Iceland and Newfoundland 1993-1998, *J. Geophys. Res.*, 104, 29599-29611, 1999.

Richardson, P.L.,Walsh, D.W.: Mapping climatological seasonal variations of surface currents in the tropical Atlantic using ship drifts, *J.Geophys. Res.*, 91, 10537-10550, 1986.

Figure Captions:

Fig. 1. Annual average sea surface salinity from (a) a climatology by Levitus et al. (1994), (b) from the model simulation (using COADS forcing). Contour interval is 0.5psu.

Fig. 2. Spatial distribution of seasonal standard deviation from (a) a climatology by Levitus et al (1994) (b) from the model simulation (using COADS forcing). Contour interval is 0.1 psu.

Fig. 3. Seasonal evolution of subpolar areal average [40N-60N, 40W-60W] SSS from a climatology (thick solid) and from a model simulation (thin), the axis is on left. Also P-E from the same area is displayed in km3, axis on right.

Fig. 4. Spatial distribution of the non-seasonal standard deviation (a), its interannual and shorter term component (periods < 4 years) (b), and its low-frequency component (periods > 4 years). Contour interval is 0.1 psu.

Fig. 5. Monthly distribution of SSS standard deviation in the subpolar gyre from the COADS simulation.

Fig. 6. Simulated subpolar SSS in March (grey) and August (black) from a simulation using (a) COADS forcing , (b) NCEP/NCAR Reanalysis. No detrending has been applied to the SSS data.

Fig. 7. (a) March mixed layer depth versus August SSS (COADS) in the subpolar gyre. (b) March mixed layer depth anomaly in COADS (solid) and in Reanalysis (dashed) simulation in the subpolar gyre. (c) August SSS in COADS (solid) and in Reanalysis (dashed) simulation in the subpolar gyre. No detrending has been applied to the data.

Fig. 8. Population of grid points with anomalous mixed layer depth (dashed) and SSS (solid) greater than +1SD (positive values) and less than -1 SD (negative values). (a) COADS and (b) Reanalysis simulation. No detrending has been applied to the data.

Fig. 9. SSS in the NECC region: annual cycle of SSS from the climatology (solid) and model (dashed) and the simulated non-seasonal standard deviation (thin). Axis for SSS on left, and axis for standard deviation on right.

Fig. 10. Composite SSS at the extrema of MHT45 (COADS simulation) at lag 0 (a) and lag +1 year (b) after the extrema, where fields corresponding to MHT45 exceeding -1 SD are subtracted from fields corresponding to MHT45 values exceeding + 1 SD. Contour interval is 0.1 psu and the dashed regions indicate areas where the difference is statistically significant at 95% level.

Fig. 11. (a) The first EOF mode of normalized SSS. Non-dimensional contour interval is 0.1. (b) PC1 of SSS (dashed), MHT45 (thick) and averaged potential temperature in the top 500 meters (thin). All values are normalized by their respective SD. Note the reversed axis on the right for the temperature.

Fig. 12. Subpolar SSS (thick) averaged over August-October and the Denmark Strait sea ice export (thin) averaged from Jan-October of the same year. Note the reversed axis on the right for the ice export.

Fig. 13. Composite of August-October SSS at the extrema of the Denmark Strait ice export (annual values) where fields corresponding to ice export exceeding -1 SD are subtracted from fields corresponding to the export values exceeding + 1 SD. Contour interval is 0.1 psu and the dashed regions indicate areas where the difference is statistically significant at 95% level.

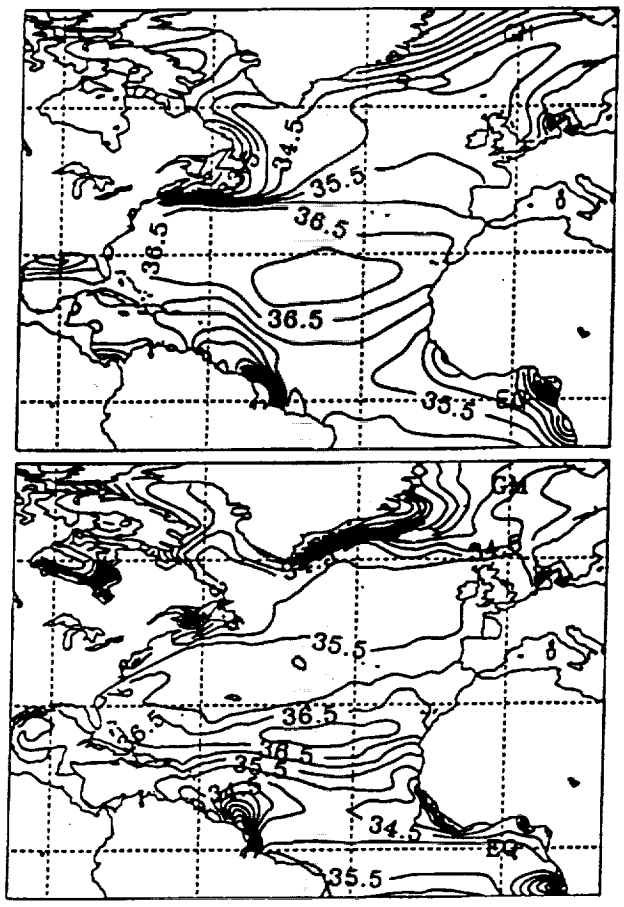

F1

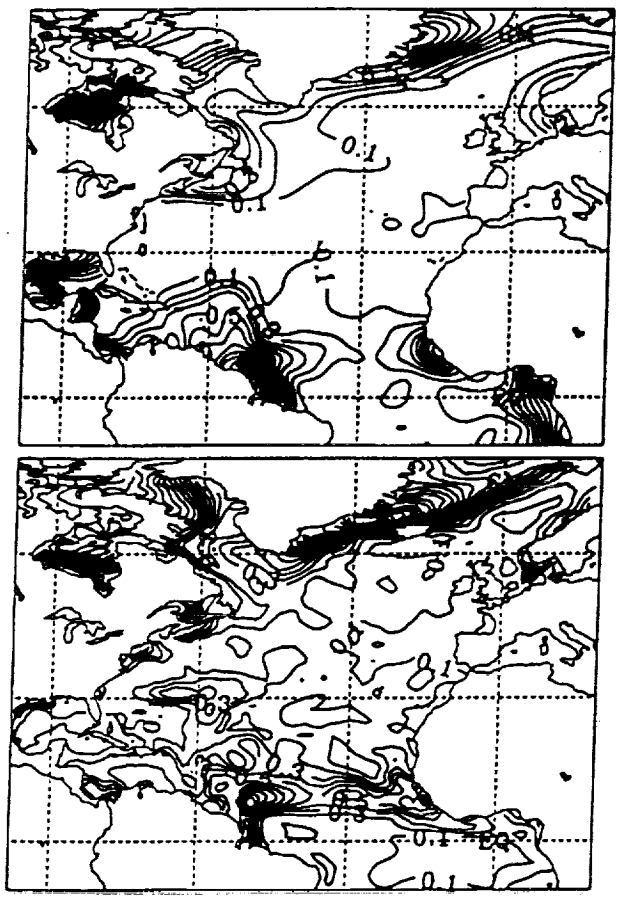

(a)

(b)

F 2

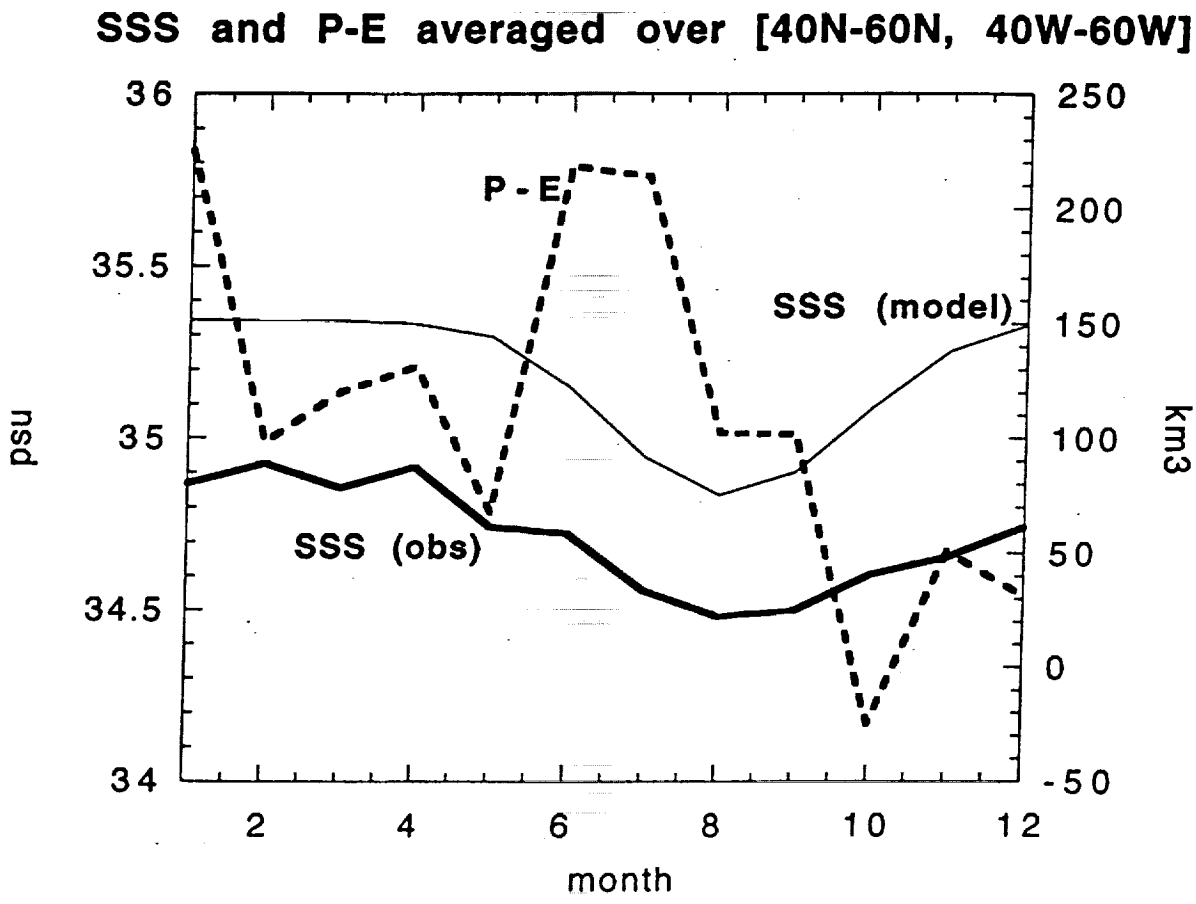
SSS and P-E averaged over [40N-60N, 40W-60W]
36
35.5
35
34.5
34
psu
250
200
150
100
50
0
-50
km3
P - E
SSS (model)
SSS (obs)
2
4
6
8
10
12
month

F3

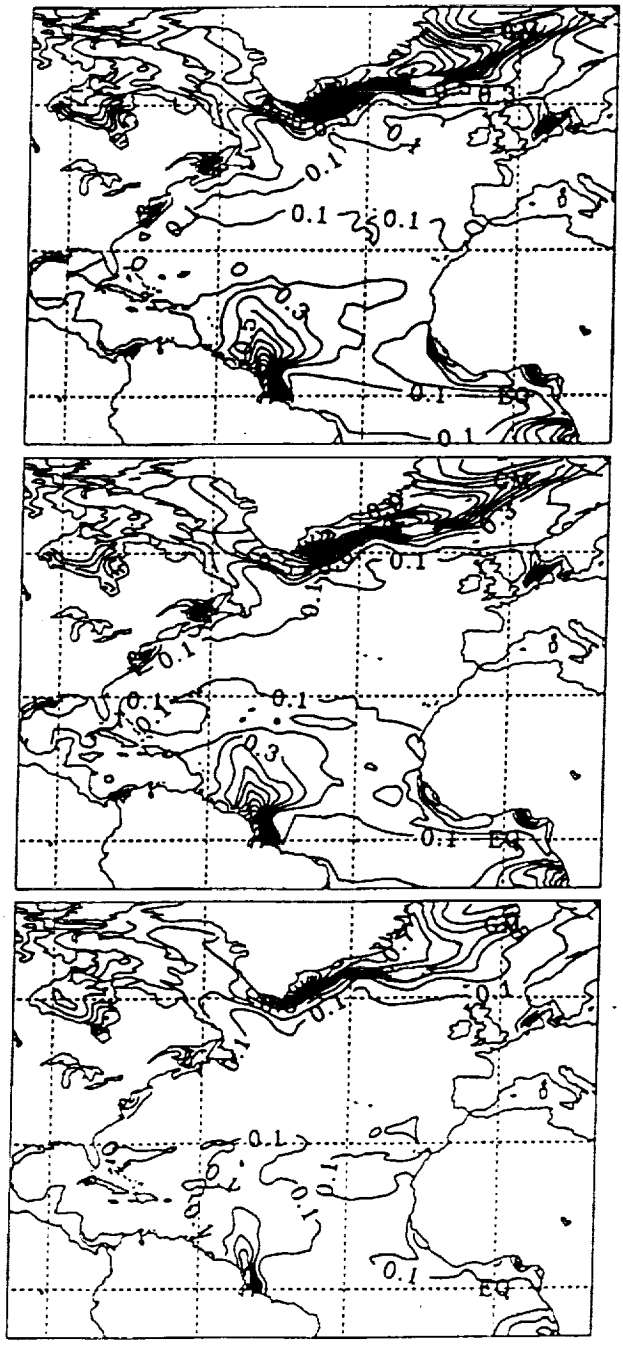

(a)

(b)

(c)

F4

MONTHLY DISTRIBUTION OF STANDARD DEVIATION OF SUBPOLAR SSS

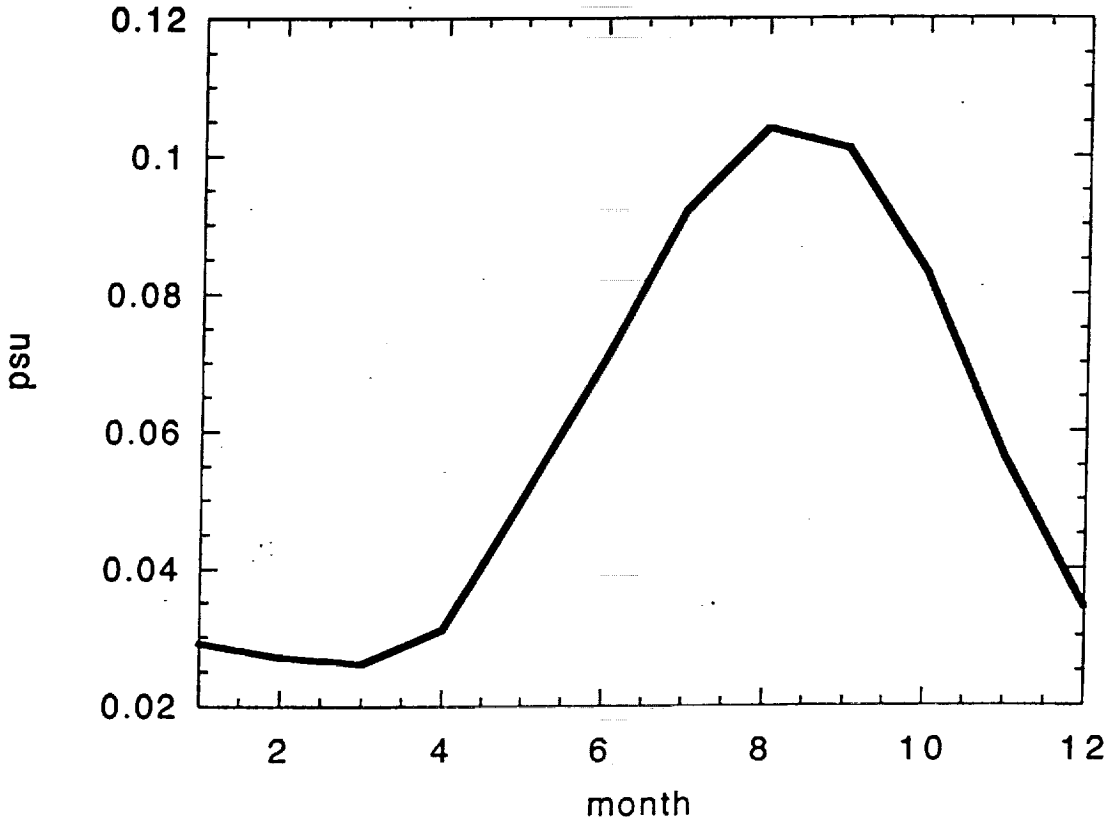

F5

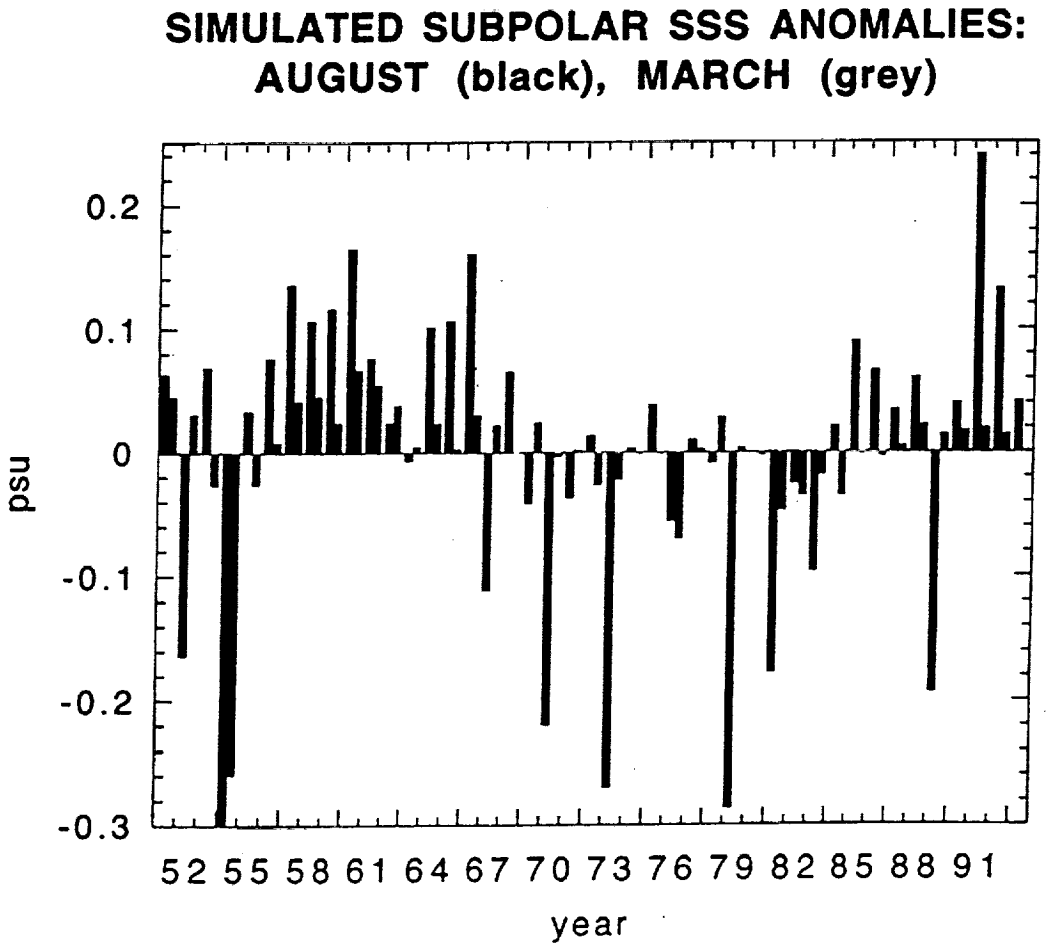
SIMULATED SUBPOLAR SSS ANOMALIES:
AUGUST (black), MARCH (grey)
0.2
0.1
0
-0.1
-0.2
-0.3
psu
52 55 58 61 64 67 70 73 76 79 82 85 88 91
year

F6a

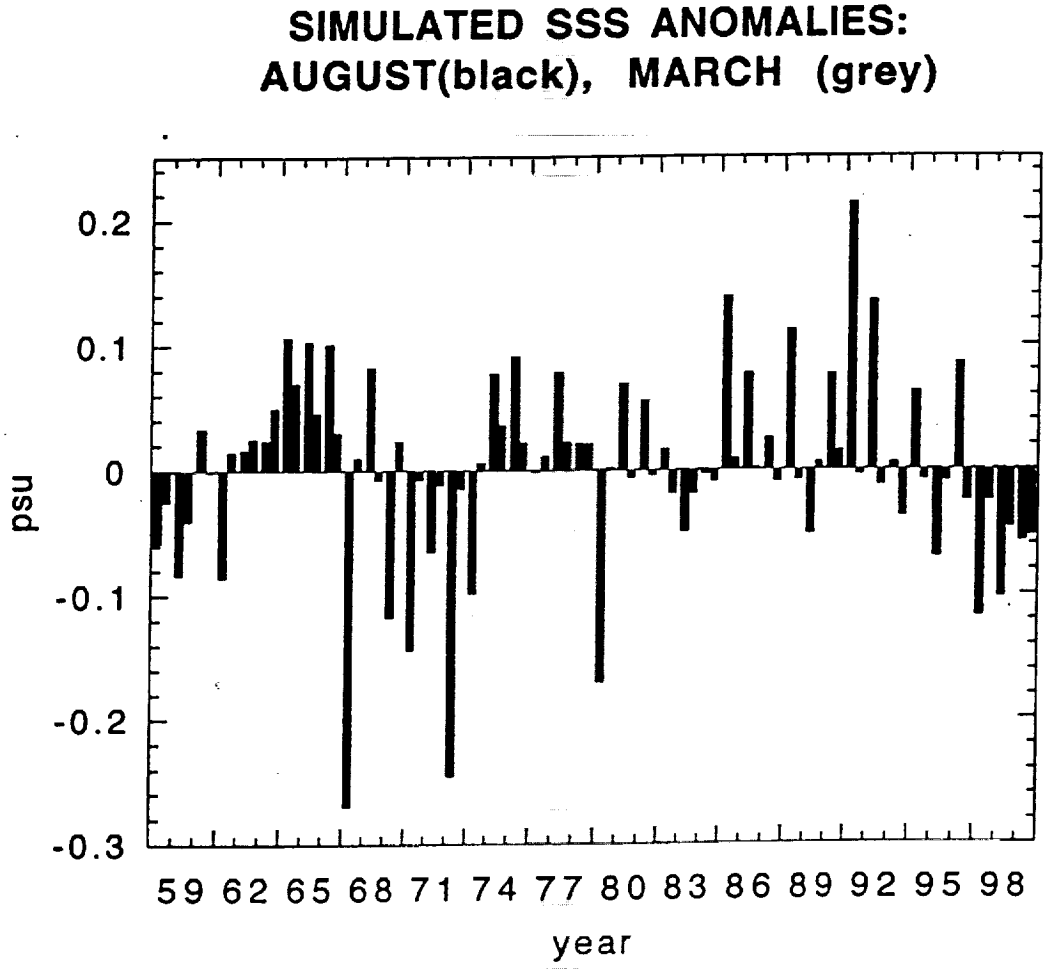
SIMULATED SSS ANOMALIES:
AUGUST(black), MARCH (grey)
0.2
0.1
0
-0.1
-0.2
-0.3
psu
59 62 65 68 71 74 77 80 83 86 89 92 95 98
year

F6b

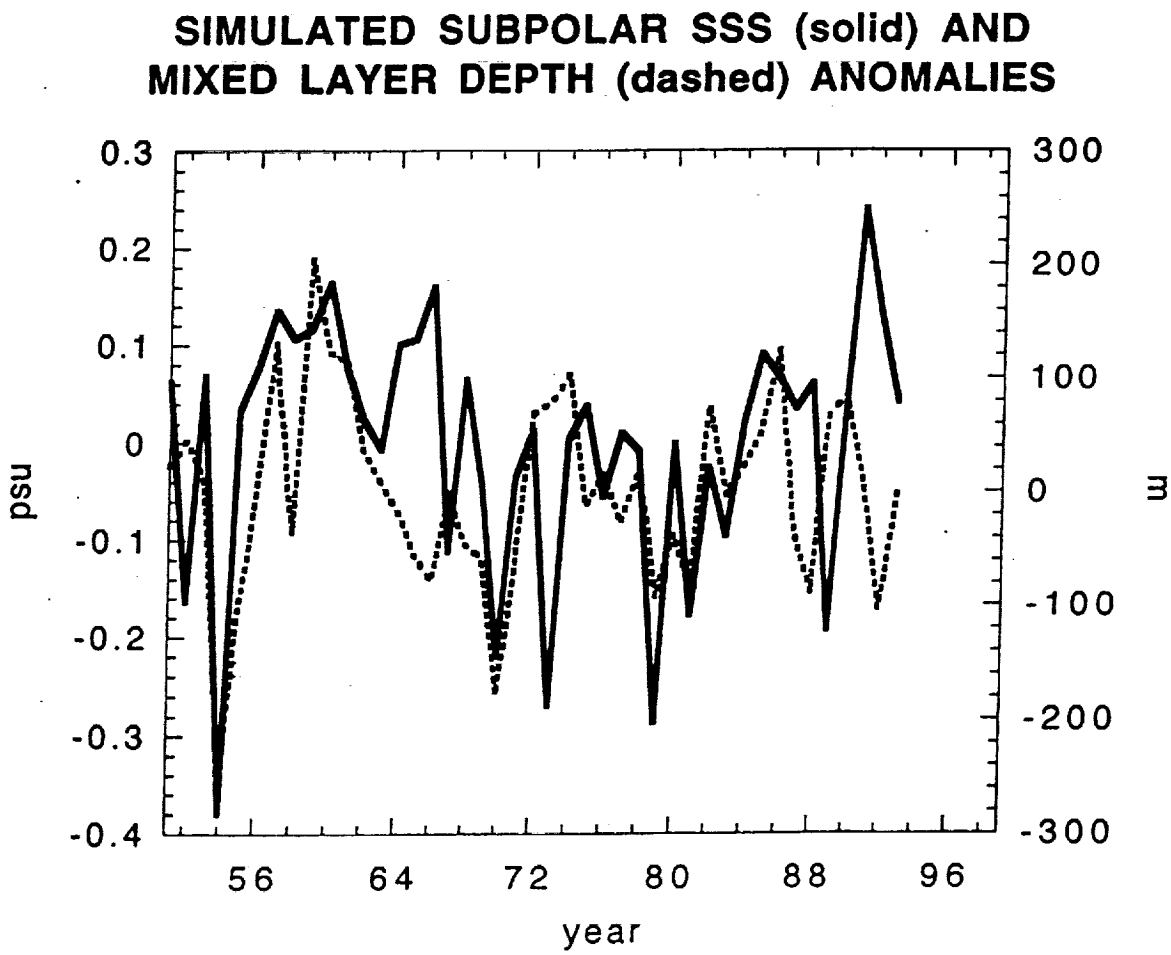
SIMULATED SUBPOLAR SSS (solid) AND
MIXED LAYER DEPTH (dashed) ANOMALIES
0.3
0.2
0.1
0
-0.1
-0.2
-0.3
-0.4
psu
300
200
100
0
-100
-200
-300
m
56
64
72
80
88
96
year

F7a

MARCH MIXED LAYER DEPTH ANOMALIES FROM COADS (solid) and NCEP (dashed) SIMULATION IN THE SUBPOLAR GYRE

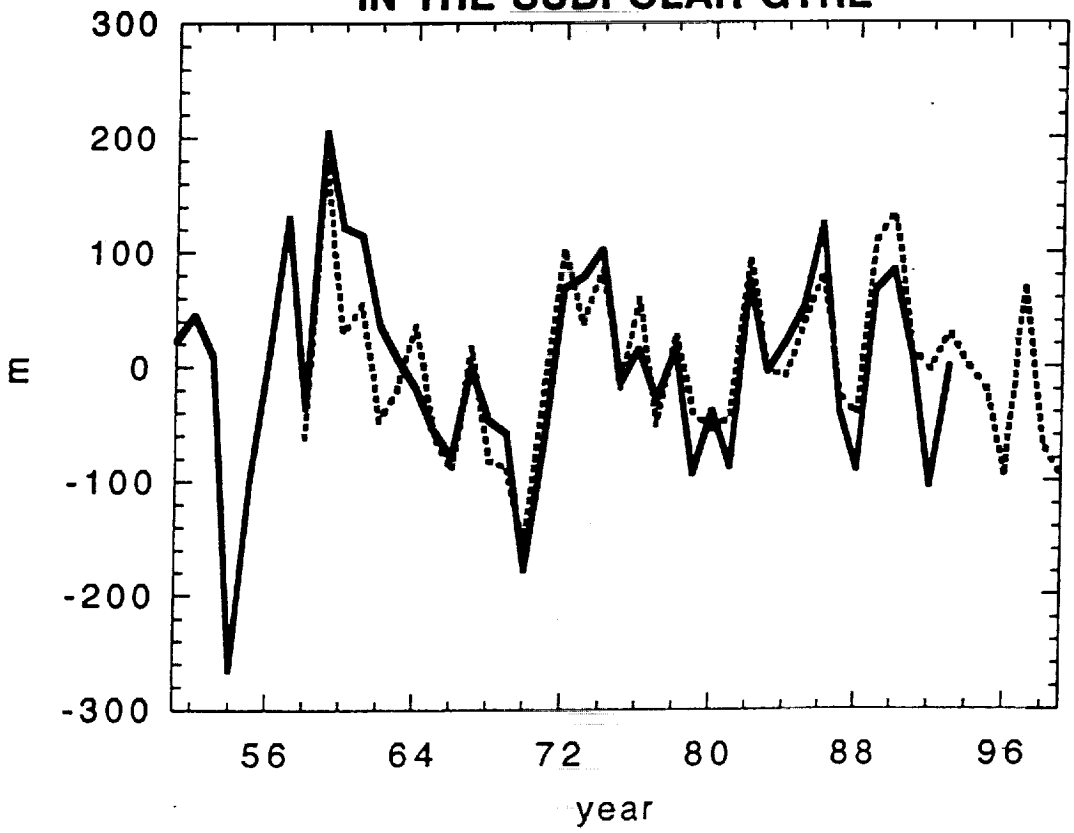

F 7b

AUGUST SSS ANOMALIES FROM COADS (solid) AND NCEP (dashed) SIMULATION IN THE SUBPOLAR GYRE

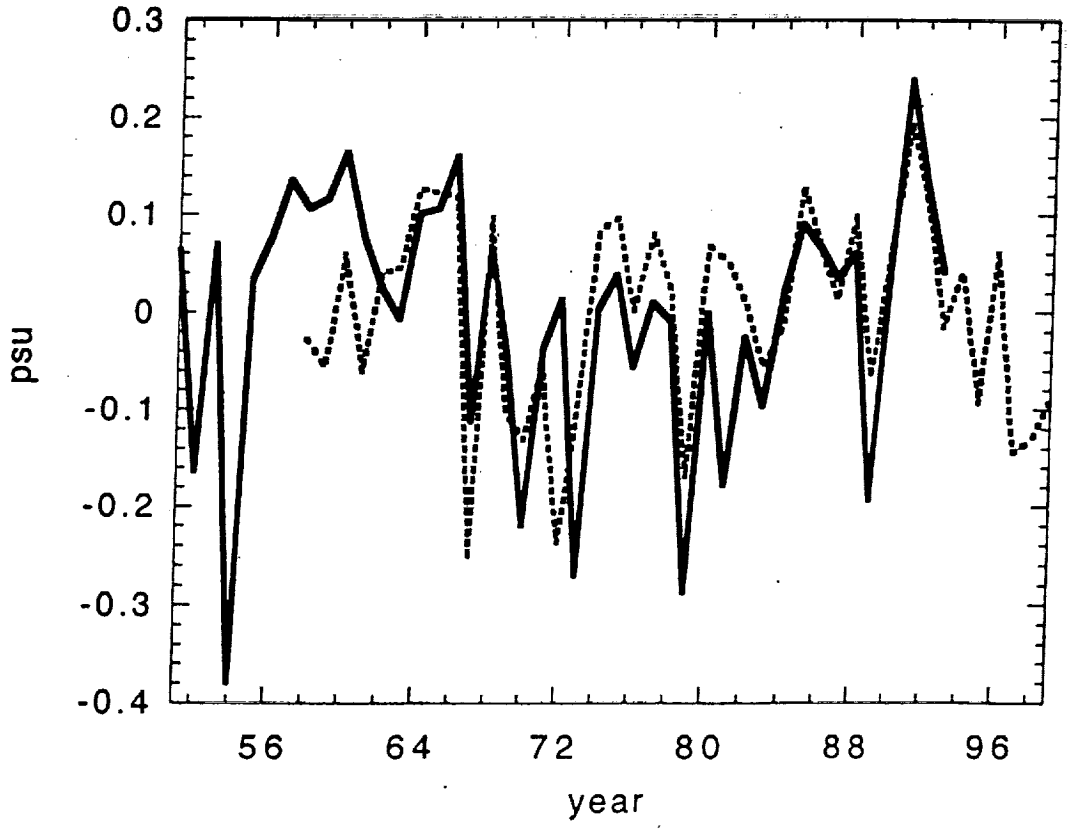

F7c

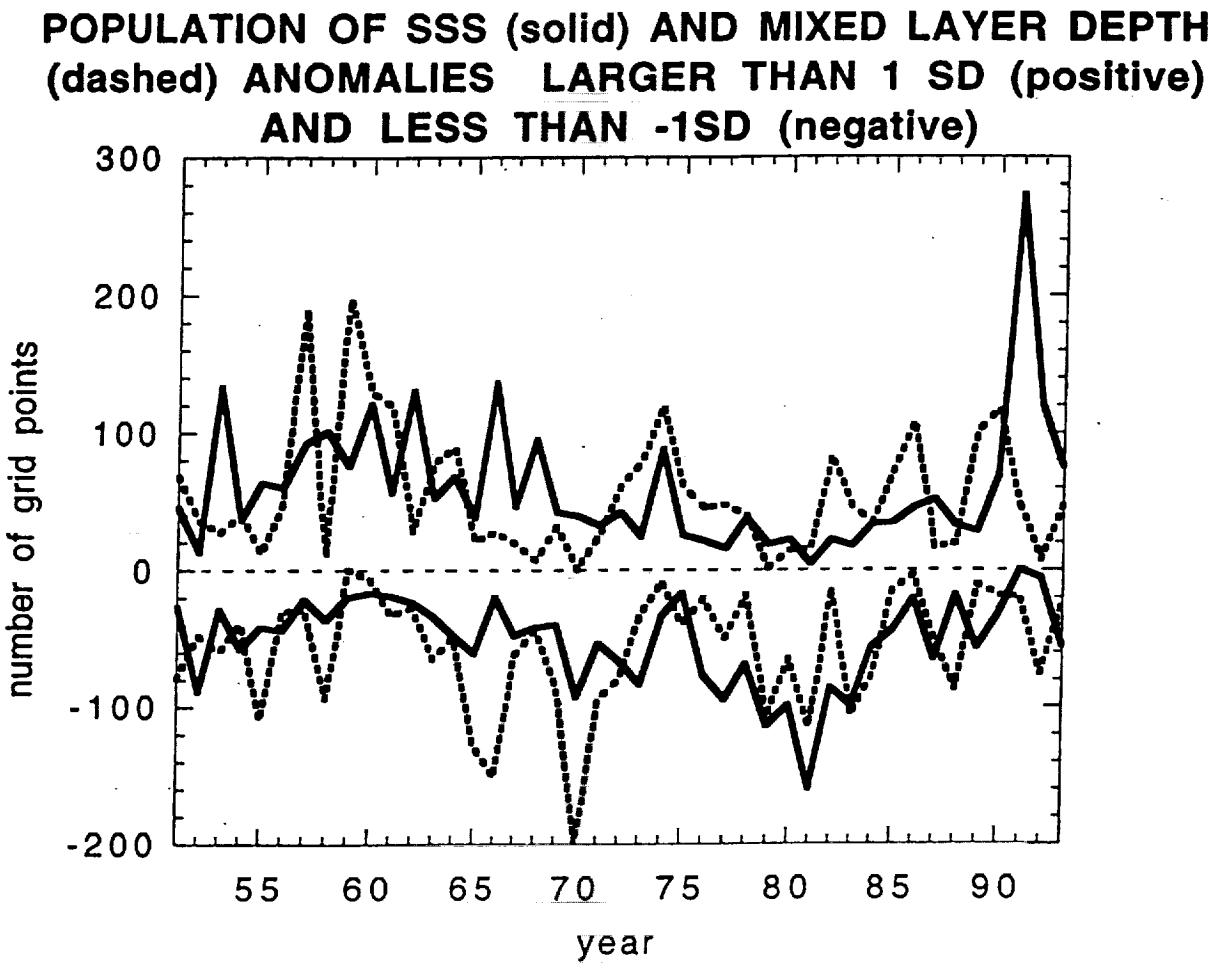
POPULATION OF SSS (solid) AND MIXED LAYER DEPTH
(dashed) ANOMALIES LARGER THAN 1 SD (positive)
AND LESS THAN -1SD (negative)
300
200
100
0
-100
-200
number of grid points
55
60
65
70
75
80
85
90
year

F8a

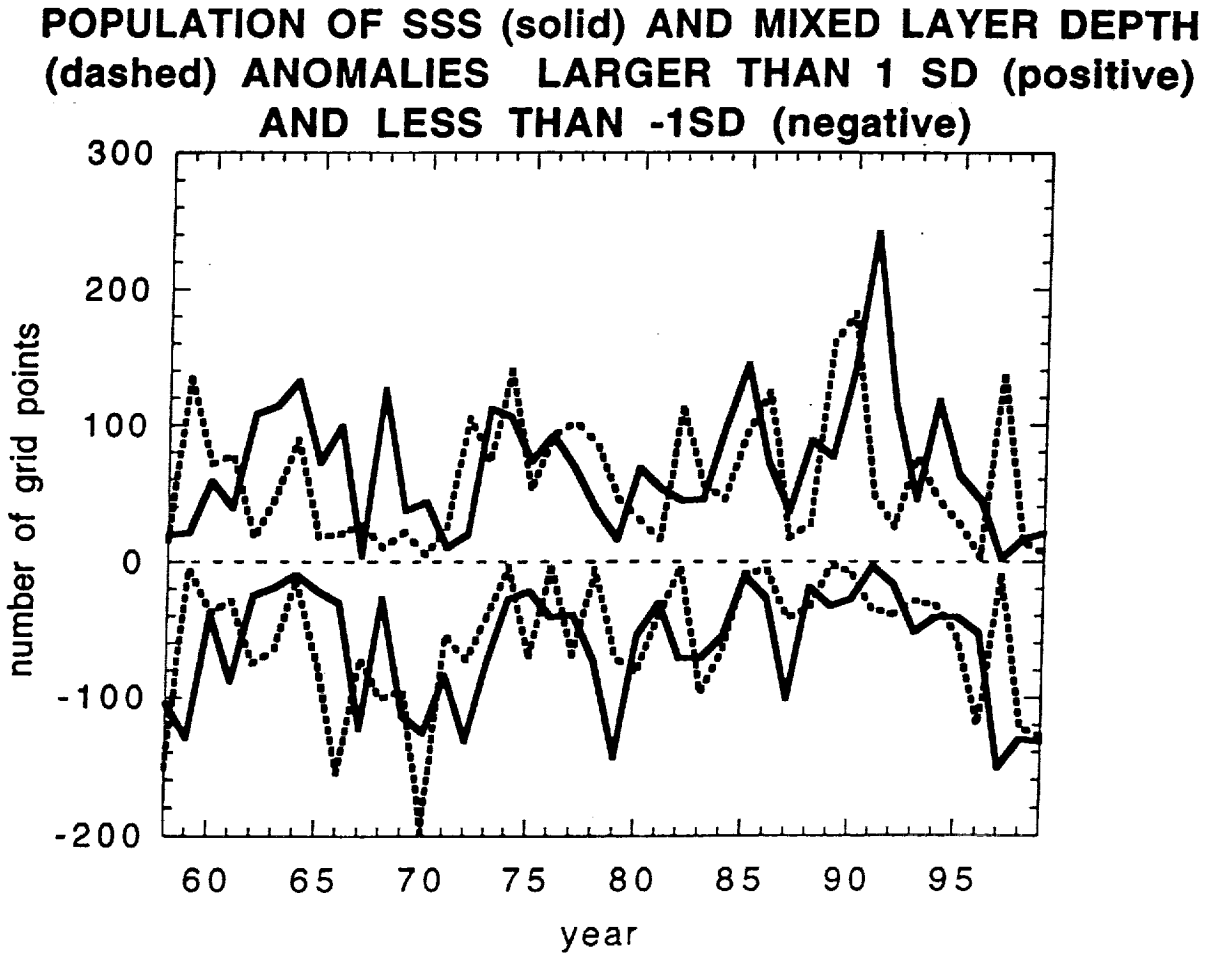
POPULATION OF SSS (solid) AND MIXED LAYER DEPTH
(dashed) ANOMALIES LARGER THAN 1 SD (positive)
AND LESS THAN -1SD (negative)
300
200
100
0
-100
-200
number of grid points
60
65
70
75
80
85
90
95
year

F 8b

SSS IN NECC REGION FROM CLIMATOLOGY (thick) SIMULATION (dashed) AND ITS SIMULATED MONTHLY DISTRIBUTION OF STANDARD DEVIATION (thin)

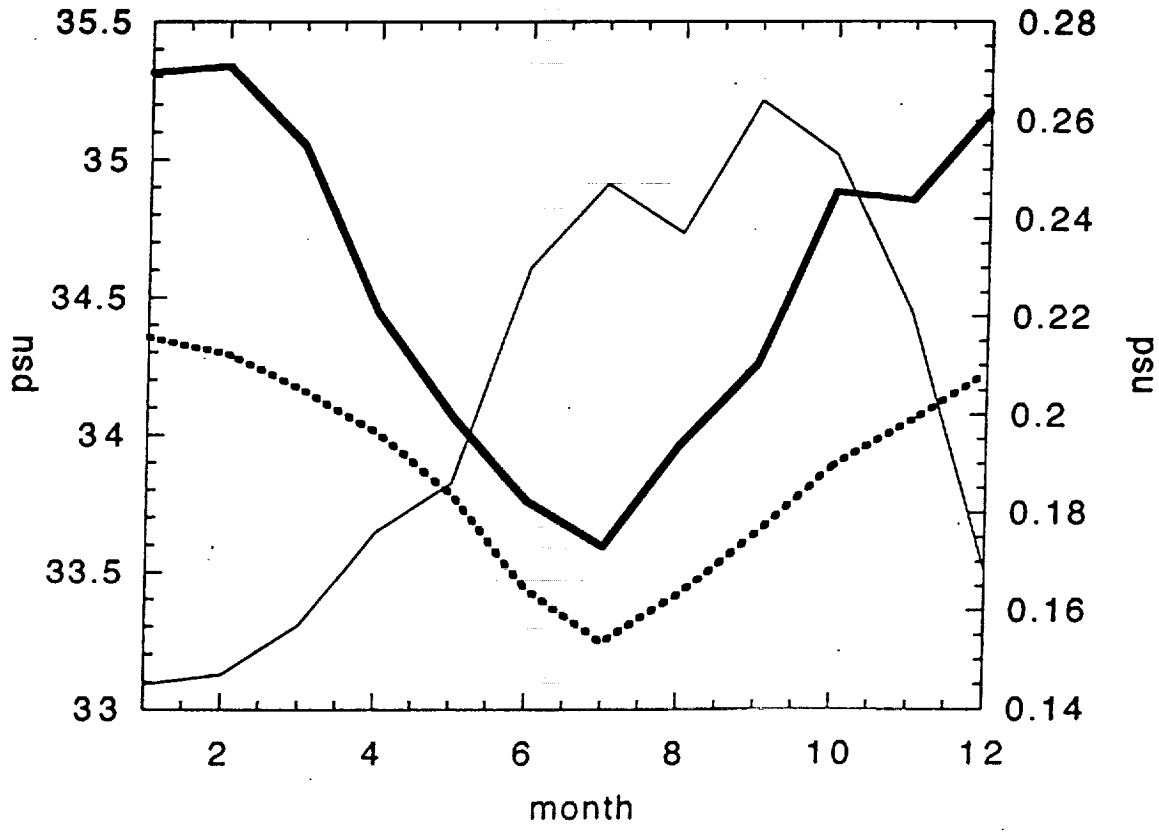

F9

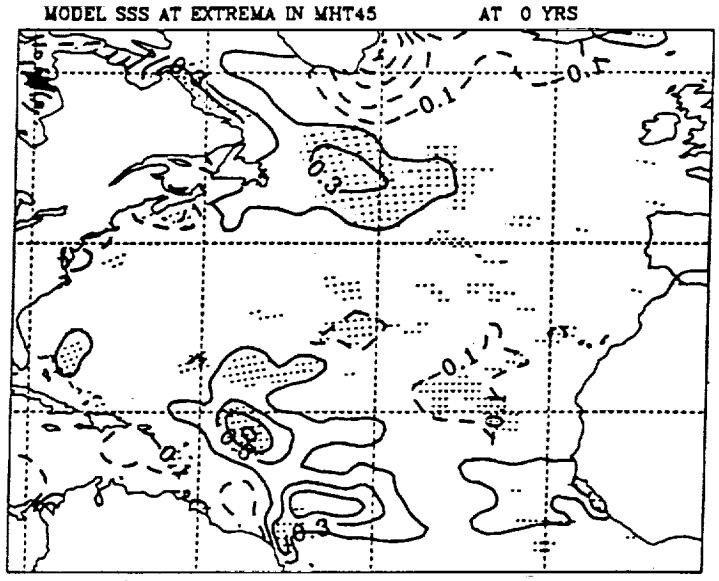
MODEL SSS AT EXTREMA IN MHT45
AT 0 YRS
0.5
0.1
0.3
-0.1
0.3

(a)

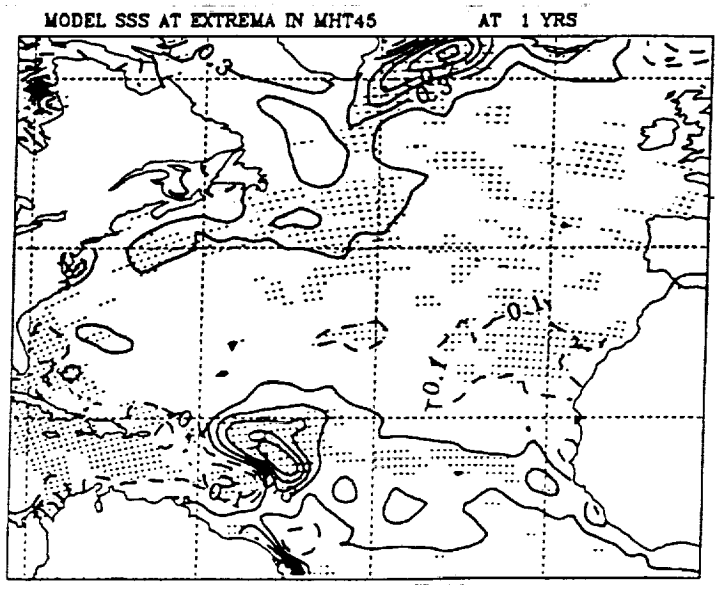
MODEL SSS AT EXTREMA IN MHT45
AT 1 YRS
0.3
-0.1
0.1

(b)

F10

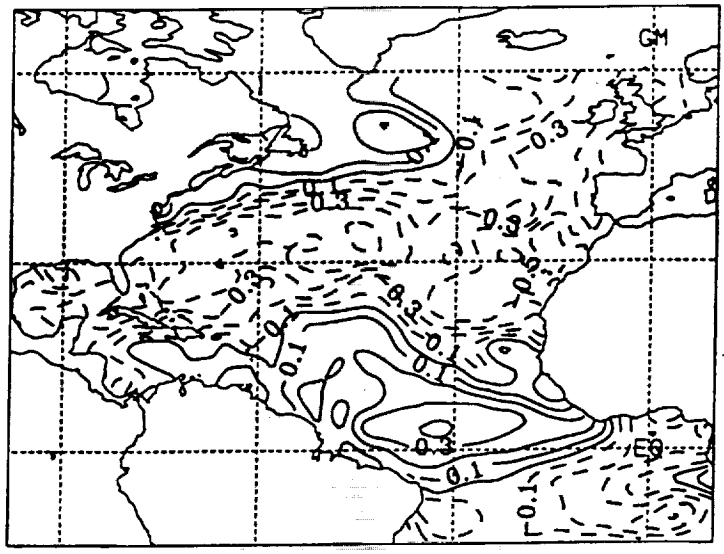

Fila

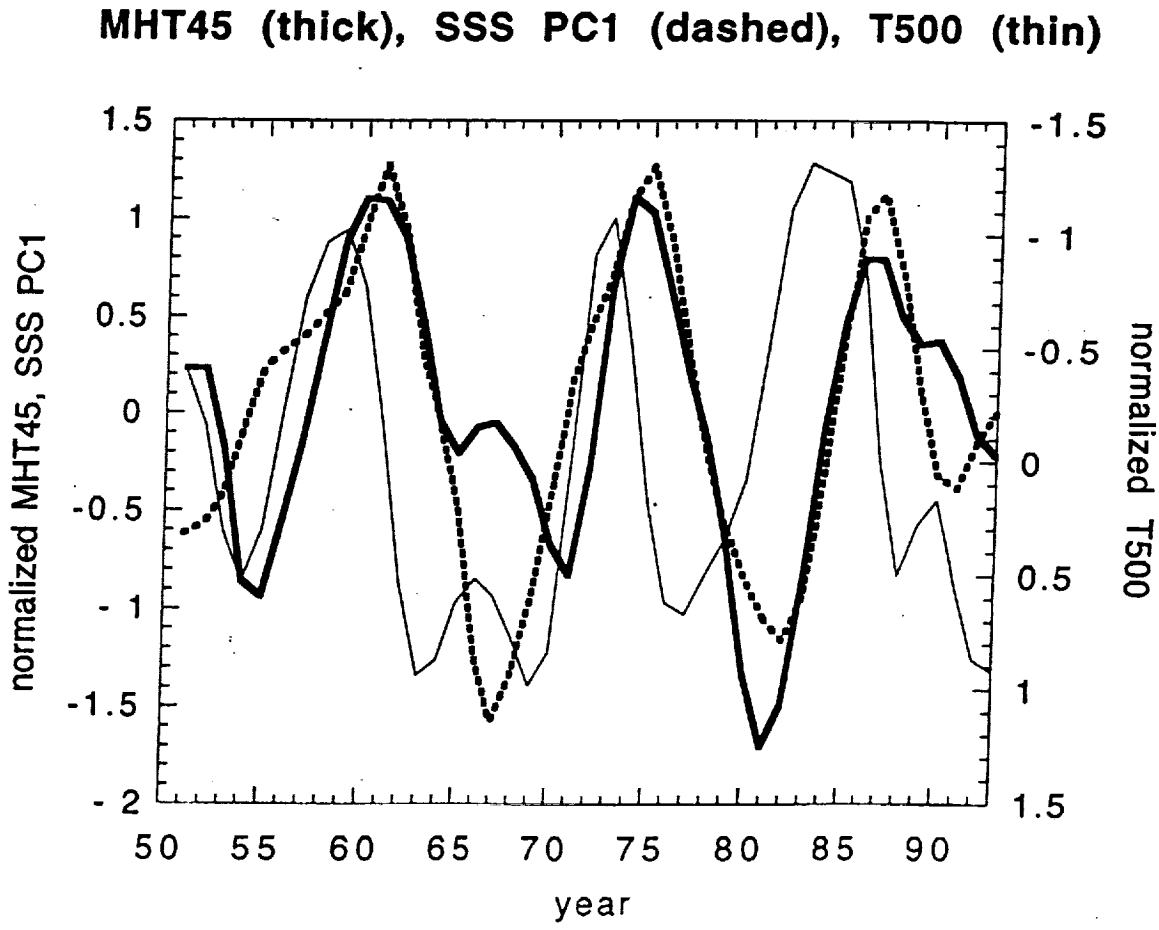
MHT45 (thick), SSS PC1 (dashed), T500 (thin)
normalized MHT45, SSS PC1
normalized T500
year
1.5
1
0.5
0
-0.5
- 1
-1.5
- 2
-1.5
- 1
-0.5
0
0.5
1
1.5
50
55
60
65
70
75
80
85
90

F11b

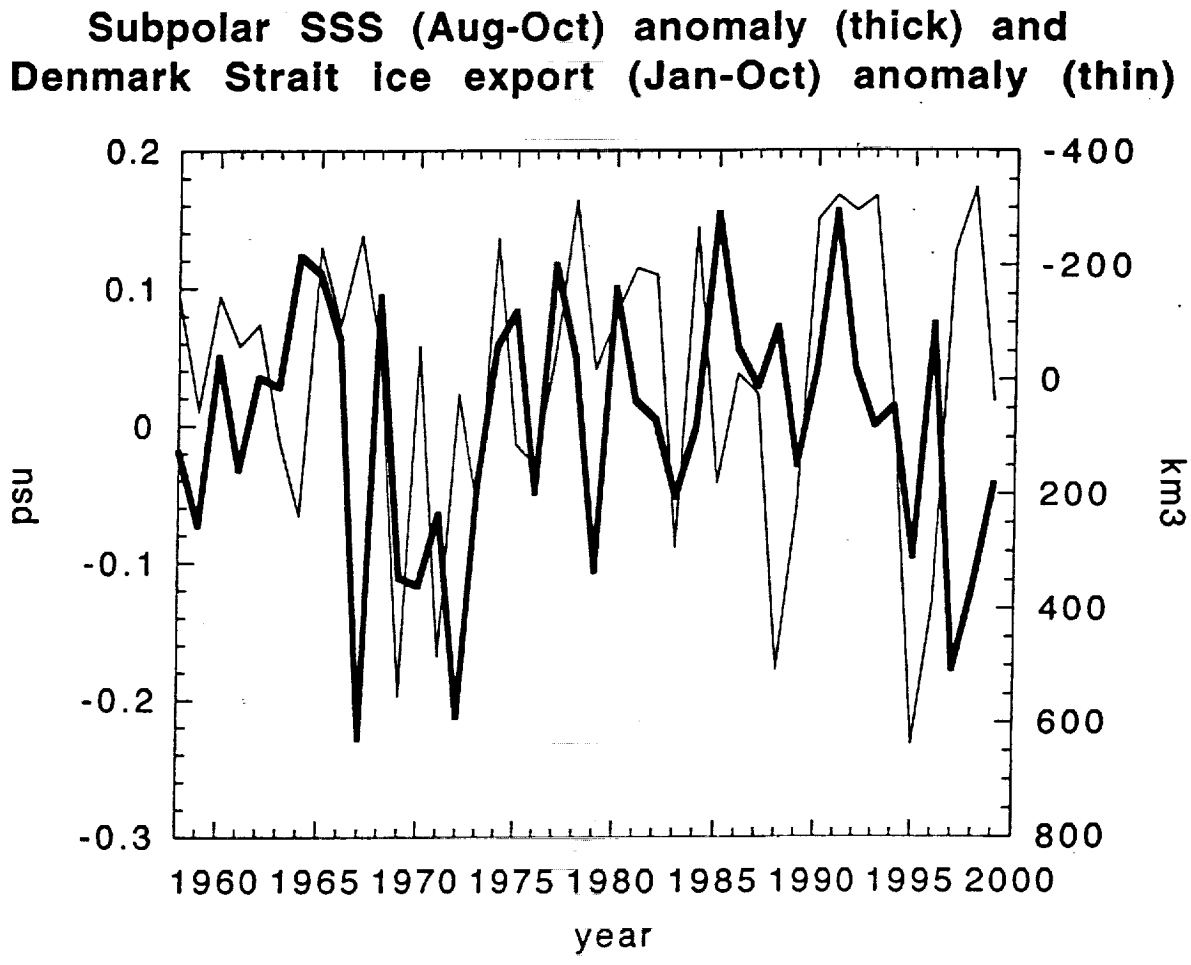
Subpolar SSS (Aug-Oct) anomaly (thick) and
Denmark Strait ice export (Jan-Oct) anomaly (thin)
0.2
0.1
0
-0.1
-0.2
-0.3
psu
-400
-200
0
200
400
600
800
km3
1960 1965 1970 1975 1980 1985 1990 1995 2000
year

F12

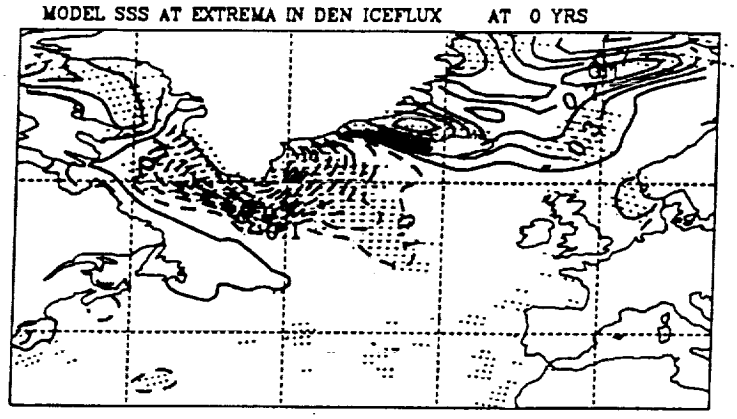
MODEL SSS AT EXTREMA IN DEN ICEFLUX AT 0 YRS

(a)

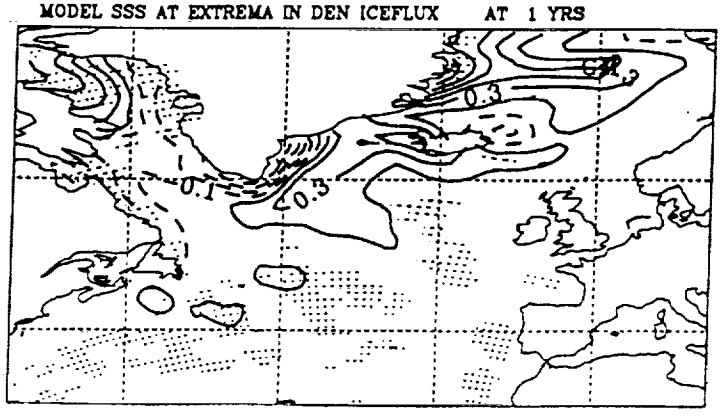
MODEL SSS AT EXTREMA IN DEN ICEFLUX AT 1 YRS
0.1
0.3
0.3

(b)

F13